SCULLING AND SCROLLING EFFECTS ON THE PERFORMANCE OF MULTIRATE TERRESTRIAL STRAPDOWN NAVIGATION ALGORITHMS

Jacques Waldmann
Instituto Tecnológico de Aeronáutica - Department of Systems and Control - 12228-900 - São José dos Campos - SP - Brazil
e-mail: jacques@ele.ita.br

Abstract. This paper investigates potential gains in velocity and position estimation accuracy promoted by sculling and scrolling corrective terms in Savage´s multirate terrestrial strapdown navigation algorithm in comparison with Bar-Itzhack´s b-l approach. Both employ inertial angular and velocity incremental output provided at a fast rate by strapdown accelerometers and rate gyros, respectively. The former algorithm transforms the thrust velocity increments at an intermediate rate from the body coordinate frame to local level to obtain ground velocity. The computations are quite complex due to sculling and scrolling corrections. A modified, discrete-time version of Bar-Itzhack´s b-l algorithm solves the whole thrust velocity at a fast rate entirely in the body frame, whereas the gravitation-induced ground velocity is solved in the local-level frame at an intermediate rate. The results show the latter approach, though significantly simpler than Savage's, yields comparable accuracy. The interaction between sensor quantization and sampling frequency is also investigated to ascertain the validity of Savage´s proposed model of sensor quantization based on white noise differentiation; a theoretical flaw in such a model is briefly highlighted. Finally, simulation results show that the error behavior is not as predicted by such a model.

Keywords. strapdown inertial navigation, navigation error, autonomous vehicles, robotics

1. Introduction

Unmanned vehicles are expected to navigate autonomously in an unstructured environment. For that purpose, such vehicles are equipped with a strapdown inertial navigation system (SDINS) that provides position and velocity with acceptable accuracy during a period of time. Among the advantages of the SDINS, one can point out that it is self-contained, obviates irradiation to and/or collection of energy from the environment, is suitable for autonomous navigation tasks by robotic vehicles, and is naturally hardened to jamming. Unfortunately, the navigation errors grow unbounded if left unchecked by external aids.

Recently, forced singular perturbations (FSP) have found a novel application as a theoretical setting to intuitive, physically sound assumptions used to derive multirate terrestrial navigation algorithms (Waldmann, 2003a, 2003b; Savage, 1998; Bar-Itzhack, 1977, 1978). These algorithms reduce the computational burden by numerically integrating the navigation equations at different rates. Analogously, FSP reduces the full-order system complexity by artificially separating the state components into distinct boundary layers. As a result, smaller interconnected dynamical systems arise, and a distinct solution to each fast variable is sought in each time scale. The purpose of the multirate approach is to match the computational workload of the navigation algorithm to the limited computational resources on board the autonomous vehicle, while extracting the rich information content embedded in inertial data acquired at a fast rate.

Here, an investigation of the attained navigation accuracy is carried out in the discrete-time domain between a modified version of Bar-Itzhack's b-l split-coordinate multirate scheme and Savage´s approach to multirate strapdown algorithms. The former solves the thrust velocity entirely in the body coordinate frame at a fast rate and transforms it to local level when position and ground velocity are required. Contrastingly, the latter transforms thrust velocity increments from the body frame to local level, and solves the ground velocity at an intermediate rate. The latter approach includes complex compensation terms to attenuate sculling- and scrolling-induced errors that arise from the rotation of body and local-level frames between consecutive inertial data samples, velocity and position updates.

In this work, sensor frequency response was assumed to be perfect. Hence, the attitude algorithms address neither nonideal gyro frequency response nor filtered gyro data (Mark, 2001). However, the interaction between sensor quantization error and measurement frequency was investigated. This investigation is relevant after claims by Savage (2002) that have contradicted simulation results obtained by Musoff (1995). The former stated that quantization-induced errors decrease with raising measurement frequency, whereas the latter claimed an increase. Savage's work asserted a continuous-time derivative of white noise is a meaningful model of quantization-induced navigation error attenuation caused by increasing sensor sampling frequency. Neither observations nor simulation results were presented to validate such unusual model; no mention made to the mathematical fact that white noise is nondifferentiable. This investigation aims at determining whether quantization-induced navigation errors behave in agreement with Savage's assertions.

Before proceeding, a few remarks are in order regarding the relevance of this work:

1 - The original derivation of multirate strapdown algorithms was proposed by Bar-Itzhack (1977, 1978) but no results have been reported concerning the b-l split coordinate-frame. The subject of multirate algorithms was further pursued and thoroughly described from a different perspective by Savage (1998), as well as by Litmanovitch *et al.* (2000). The aggregation of strapdown navigation dynamics into time scales based on intuitive, physical reasoning was assumed to reduce the computations.

2 - It has been argued that the computational load as one of the criteria in the evaluation of algorithm performance is not meaningful because of modern computers with increasing throughput (Savage, 1998; Litmanovitch, 2000). However, one should realize that the latest electronics onboard myriad autonomous systems, ranging from satellites to

robotic soccer players to miniature unmanned air vehicles must be qualified with regards to vibration levels, energy consumption, temperature variations, vacuum conditions when applicable, and electromagnetic interference in the expected operating conditions. Hence, less sophisticated though already qualified equipment is often employed because of the complexity, costs, and time involved in qualification procedures.

3 - The navigation solution is but one more task to share available resources according to the priorities dictated by the real-time system onboard. The history of real-time computing reveals that the demand for more computing power has always outpaced the supply. More computing power raises the need for novel real-time applications that in turn require more functionality, hence aggravating the timing constraints (Stankovic, 1988). Actually, design for predictability and meeting specifications at acceptable costs should be the foremost goal. Hence, there is no substitute for a smart deployment of finite computational resources. In real-time system design, one should allocate resources to ensure that critical timing constraints can be met with the available resources in the expected operating conditions. Although there is no guarantee that such conditions will not be violated, this uncertainty does not give the software designer a license to increase the odds of failure by not trying to allocate resources carefully to meet the timing constraints. The reliability of the real-time computer system in meeting timing constraints depends heavily on its workload; hence, the the relevance of guidance and navigation algorithms that reduce the computational workload.

2. Overview of the discrete-time b-l split-coordinate computational scheme

Following Bar-Itzhack's notation (1977, 1978), vector quantities are in bold font. The centered superscript on top a vector denotes the coordinate frame in which a time derivative is observed, and a right-hand subscript expresses the coordinate frame used to represent the vector. Consider a vehicle that rotates and translates relative to coordinate frame S_e fixed to the rotating earth, and let S_l denote the local-level North-East-Down (NED) coordinate frame that accompanies the vehicle's translation. One is interested in estimating the geographic latitude, longitude, and altitude position coordinates, λ, Λ, and h, respectively, of the position vector $\mathbf{R}$ relative to the center of the earth, and ground velocity $\mathbf{U} = \overset{e}{\mathbf{R}}$ represented in the local-level frame, i.e., $\mathbf{U}_l = \begin{bmatrix} V_N & V_E & V_D \end{bmatrix}^T$. The vehicle is equipped with strapdown accelerometer and rate gyro triads aligned with the body coordinate frame S_b. The accelerometer triad measures the specific force $\mathbf{f}$ acting on the vehicle relative to the inertial frame S_i, represented in the body coordinate frame:

$$\mathbf{f_b} = \overset{ii}{\mathbf{R}_b} - \mathbf{g_{m,b}} \tag{1}$$

where $\mathbf{g_{m,b}}$ is the local gravitation vector coordinatized in the body frame, and

$$\mathbf{g_{m,b}} = \mathbf{D_b^l}(\mathbf{g_l} + [\mathbf{\Omega_l}]^2 \mathbf{D_l^e} \mathbf{R_e}); \quad \mathbf{\Omega_l} = \mathbf{\omega_l^{ei}} = \begin{bmatrix} \Omega c\lambda & 0 & \Omega s\lambda \end{bmatrix}^T \quad \mathbf{g_l} = \begin{bmatrix} 0 & 0 & g(\lambda,h) \end{bmatrix}^T$$

$$[\mathbf{\Omega_l}] = \begin{bmatrix} 0 & \Omega\sin(\lambda) & 0 \\ -\Omega\sin(\lambda) & 0 & -\Omega\cos(\lambda) \\ 0 & \Omega\cos(\lambda) & 0 \end{bmatrix} \tag{2}$$

where $[\mathbf{\Omega_l}]$ is the antisymmetric matrix representation of the vector product operation with earth's angular rate $\mathbf{\Omega_l}$, $g(\lambda,h)$ is the local-level gravity magnitude modeled by the U.S. DoD World Geodetic System WGS-84, and $\mathbf{D_y^x}$ is the direction cosine matrix (DCM) transforming from coordinate frame S_x to S_y. The accelerometers output inertial velocity increments between consecutive sensor samples:

$$\Delta\mathbf{\beta_b} = \int_{(k-1)T_{gyr}}^{kT_{gyr}} \mathbf{f_b}(\tau)d\tau \tag{3}$$

where T_{gyr} is the inertial sensor acquisition period. Likewise, the rate gyros output inertial angular increments:

$$\Delta\mathbf{\phi_b} = \int_{(k-1)T_{gyr}}^{kT_{gyr}} \mathbf{\omega_b^{bi}}(\tau)d\tau \tag{4}$$

The above right-hand superscript denotes the angular rate of the body coordinate frame relative to the inertial frame. Furthermore, let $\mathbf{\rho} = \mathbf{\omega^{le}}$ denote the angular rate of S_l relative to S_e, with representation in S_l given by:

$$\mathbf{\rho_l} = \begin{bmatrix} \dot{\Lambda}c\lambda & -\dot{\lambda} & -\dot{\Lambda}s\lambda \end{bmatrix}^T$$
$$\dot{\lambda} = V_N / [R_N(\lambda) + h]$$

$$\dot{\Lambda} = V_E / \{[R_E(\lambda) + h]\cos(\lambda)\} \tag{5}$$

R_N and R_E are the reference ellipsoid north and east curvature radii from WGS-84, respectively. The guideline to multirate algorithms Bar-Itzhack (1977, 1978) advocates is to perform as few computations as possible at a fast rate in the rapidly rotating body coordinate frame. For this purpose, it is useful to decompose both ground velocity $\mathbf{U}$ and inertial velocity $\mathbf{V} = \overset{i}{\mathbf{R}}$ as follows:

$$\mathbf{V} = \mathbf{U} + \boldsymbol{\Omega} \times \mathbf{R}; \ \mathbf{V_b} = \mathbf{V_{f,b}} + \mathbf{V_{g,b}} \tag{6}$$

$$\mathbf{U_l} = \mathbf{U_{f,l}} + \mathbf{U_{g,l}} \tag{7}$$

$\mathbf{V_{f,b}}$ is the inertial thrust velocity component due to all nongravitational forces acting on the vehicle with zero initial condition, whereas $\mathbf{V_{g,b}}$ is caused by gravitational forces in addition to the vehicle's initial inertial velocity $\mathbf{V_b}(0)$. Similarly, one has for ground velocity $\mathbf{U_{f,l}}$ ($\mathbf{U_{g,l}}$) accounting for the effects of nongravitational (gravitational) forces and its initial condition $\mathbf{U_{f,l}}(0)=\mathbf{0}$ ($\mathbf{U_{g,l}}(0)=\mathbf{U_l}(0)$). The multirate scheme calls for a fast computation-cycle period T_{gyr} that captures the information content of body-fixed rapidly varying inertial data to accurately update thrust velocity $\mathbf{V_{f,b}}$. Likewise, the intermediate cycle period T_{int} to compute the gravitation-induced component of ground velocity $\mathbf{U_{g,l}}$, and the slow navigation refresh period T_{nav}. The discrete-time multirate algorithm with vertical damping shown in Tab. (1) results from an Euler approximation to its original differential form, and includes altimeter-based vertical-channel stabilization. Linear and angular increments $\boldsymbol{\Delta\beta_b}$ and $\boldsymbol{\Delta\phi_b}$, respectively, output at a fast rate by the inertial sensors are processed in a straightforward manner. The algorithm results from a judicious selection of initial conditions, reset commands, and parameters T_{gyr}, T_{int}, and T_{nav} that weighs limited computer throughput against assumptions inherent to forcing the problem into distinct time scales (Waldmann, 2003a, 2003b; Bar-Itzhack, 1977, 1978).

Table 1 – Discrete-time modified b-l split-coordinate computational scheme

Computation rate	Navigation and attitude equations	Initial conditions	Algebraic relations and reset commands
Fast (T_{gyr})	$\mathbf{V_{f,b}}(k+1) = \mathbf{V_{f,b}}(k) - [\boldsymbol{\Delta\phi_b}(k)]\mathbf{V_{f,b}}(k) + \boldsymbol{\Delta\beta_b}(k)$ Relative quaternion update $\qquad\qquad (8)$	$\mathbf{V_{f,b}}(0)=\mathbf{0}$	$\mathbf{V_{f,b}}(k)$ reset to $\mathbf{0}$ every T_{nav}
Intermediate (T_{int})	$\mathbf{U_{g,l}}(k+1) = \mathbf{U_{g,l}}(k) + T_{int}\{-[2\boldsymbol{\Omega_l}(k) + \boldsymbol{\rho_l}(k)]\mathbf{U_{g,l}}(k) +$ $+ \mathbf{g_l}(\mathbf{R}(k)) + \mathbf{s''}(h(k))\}$	$\mathbf{U_{g,l}}(0)=\mathbf{U_l}(0)$	$\mathbf{U_{g,l}}(k)=\mathbf{U_l}(k)$ every T_{nav}
Slow (T_{nav})	$\lambda(k+1) = \lambda(k) + T_{nav}\{V_N(k)/[R_N(\lambda(k)) + h(k)]\}$ $\Lambda(k+1) = \Lambda(k) + T_{nav}\{V_E(k)/\{[R_E(\lambda(k)) +$ $+ h(k)]\cos(\lambda(k))\}$ $h(k+1) = h(k) + T_{nav}\{-V_D(k) + s'(h(k))\}$	$\lambda(0) = \lambda_0$ $\Lambda(0) = \Lambda_0$ $h(0) = h_0$	DCM update $\qquad (9)$ $\mathbf{U_l} = \mathbf{U_{g,l}} + \mathbf{D_l^b}\mathbf{V_{f,b}}$ $R_N = R_0(1-2e+3e\sin^2(\lambda))$ $R_E = R_0(1+e\sin^2(\lambda))$ $\mathbf{g_l}(\mathbf{R})$ from WGS-84 $\mathbf{s''}(h)=[0\ 0\ (h_{aux}-h)]^T$ $s'(h)=(h-h_{aux})$

The attitude determination algorithm (Waldmann, 2002) at the high-speed T_{gyr}-cycle is reproduced below for the sake of completeness:

$$\mathbf{q_b^l}(k+1) = (\mathbf{I_4} - 1/2[T_{gyr}\boldsymbol{\omega_l^{li}}(k)] + 1/2[T_{gyr}\boldsymbol{\omega_b^{bi}}(k)])\mathbf{q_b^l}(k); \ k = 1,2,3,... \ ; \ \mathbf{q_b^l}(0) \text{ given by initial alignment procedure.}$$

$$-[T_{gyr}\boldsymbol{\omega_l^{li}}(k)] = \begin{bmatrix} 0 & (\boldsymbol{\Delta\phi_l}(k))^T \\ \hline -\boldsymbol{\Delta\phi_l}(k) & -[\boldsymbol{\Delta\phi_l}(k)] \end{bmatrix}; \ \boldsymbol{\Delta\phi_l}(k) = T_{gyr}(\boldsymbol{\Omega_l}(k) + \boldsymbol{\rho_l}(k))$$

$$[\boldsymbol{\Delta\phi_l}(k)] = T_{gyr}\begin{bmatrix} 0 & (\Omega + \dot{\Lambda}(k))\sin(\lambda(k)) & -\dot{\lambda}(k) \\ -(\Omega + \dot{\Lambda}(k))\sin(\lambda(k)) & 0 & -(\Omega + \dot{\Lambda}(k))\cos(\lambda(k)) \\ \dot{\lambda}(k) & (\Omega + \dot{\Lambda}(k))\cos(\lambda(k)) & 0 \end{bmatrix}$$

$$[T_{gyr}\boldsymbol{\omega_b^{bi}}(k)] = \begin{bmatrix} 0 & -(\boldsymbol{\Delta\phi_b}(k))^T \\ \hline \boldsymbol{\Delta\phi_b}(k) & -[\boldsymbol{\Delta\phi_b}(k)] \end{bmatrix}; \ \boldsymbol{\Delta\phi_b}(k) = \begin{bmatrix} \Delta\phi_{bx}(k) \\ \Delta\phi_{by}(k) \\ \Delta\phi_{bz}(k) \end{bmatrix}; \ [\boldsymbol{\Delta\phi_b}] = \begin{bmatrix} 0 & -\Delta\phi_{bz}(k) & \Delta\phi_{by}(k) \\ \Delta\phi_{bz}(k) & 0 & -\Delta\phi_{bx}(k) \\ -\Delta\phi_{by}(k) & \Delta\phi_{bx}(k) & 0 \end{bmatrix} \tag{8}$$

where $\Delta\boldsymbol{\phi}_l$ is updated at every T_{nav}-cycle. The DCM transformation from local-level to body frame is computed once at every T_{nav}-cycle from the most recent quaternion update according to:

$$\mathbf{D}_b^l(kT_{nav}) = \begin{bmatrix} \lambda^2 + \rho_x{}^2 - \rho_y{}^2 - \rho_z{}^2 & 2(\rho_x\rho_y + \lambda\rho_z) & 2(\rho_x\rho_z - \lambda\rho_y) \\ 2(\rho_x\rho_y - \lambda\rho_z) & \lambda^2 - \rho_x{}^2 + \rho_y{}^2 - \rho_z{}^2 & 2(\rho_y\rho_z + \lambda\rho_x) \\ 2(\rho_x\rho_z + \lambda\rho_y) & 2(\rho_y\rho_z - \lambda\rho_x) & \lambda^2 - \rho_x{}^2 - \rho_y{}^2 + \rho_z{}^2 \end{bmatrix} \tag{9}$$

3. Overview of Savage´s discrete-time multirate computational scheme

Bar-Itzhack's guideline to multirate navigation algorithms design emphasizes the high-speed solution of thrust velocity in the rapidly rotating body frame, and its transformation to local level with the bulk of the computations occurring at slower rates. The theory of linear differential equations assures that splitting the computations into distinct time scales in the continuous-time domain is mathematically correct under the assumption of constant $\mathbf{g}(\mathbf{R})$ and $\boldsymbol{\rho}$ over the slow T_{nav}-cycle period. Savage´s approach, on the other hand, is inspired by two-speed approaches to attitude determination whereby an exact closed-form attitude updating operation processes at a moderate speed the results of a high-speed algorithm (Bortz, 1971; Litmanovitch, 2000; Mark, 2001; Musoff, 1995; Savage, 1998). The high-speed computations account for multiaxis high-frequency angular motion between moderate-speed algorithm updates; such motion can rectify into attitude changes traditionally denoted as coning. Analogously, accounting for attitude rotation during the velocity update time period is crucial both for accurate transformation of specific force increments from the body frame to local level and velocity update. Fot that purpose, Savage (1998) presented a two-speed approach to specific force increment transformation that paralleled two-speed attitude determination algorithms. A high-speed algorithm accounted for high-frequency angular and linear oscillations that under certain conditions rectify into systematic velocity and position changes, known as sculling and scrolling, respectively. Then, a moderate-speed algorithm accomplished the transformation of specific force increments based on results from a high-speed algorithm.

Sculling occurs when a particular combination of varying body angular rate and specific force rectifies into a net constant contribution to thrust velocity. Savage (1998) Eq. (36) showed that such a contribution is maximized under a sinusoidally varying body angular rate and specific force with the former about one S_b frame axis, at the same frequency, and in phase with the latter along another S_b frame axis. The rectified, constant thrust velocity increment thus produced lies along the average third axis direction. The term sculling originates from seamen using this very principle to propel a boat forward with a single oar operated with an undulating motion. Likewise, Savage (1998) Section C presented a high-resolution position estimation algorithm that accounted for scrolling, a term denoting a net position shift related to dynamic attitude and velocity changes within the position update period. Savage´s algorithm is reproduced below accompanied by remarks. Its complexity in comparison to that of Bar-Itzhack's approach is evident. Notice that S_{l^-} represents the local-level frame in the most recently available T_{nav}-cycle position update.

<div align="center">

High speed computations at T_{gyr}-cycle rate

($T_{int}/T_{gyr}=L$, k=1,2,...,L, k reset at every T_{int}-cycle)

</div>

1 - $\boldsymbol{\alpha}_b(k) = \boldsymbol{\alpha}_b(k-1) + \Delta\boldsymbol{\phi}_b(k); \boldsymbol{\alpha}_b(0) = \mathbf{0}; \boldsymbol{\alpha}_b(L) = \boldsymbol{\alpha}_{L,b}; \boldsymbol{\alpha}(k)$ reset at every T_{int}-cycle.

2 - $\boldsymbol{\gamma}_b(k) = \boldsymbol{\gamma}_b(k-1) + \Delta\boldsymbol{\gamma}_b(k); \boldsymbol{\gamma}_b(0) = \mathbf{0}; \boldsymbol{\gamma}_b(L) = \boldsymbol{\gamma}_{L,b}; \boldsymbol{\alpha}(k)$ reset at every T_{int}-cycle. (Coning correction)

$\Delta\boldsymbol{\gamma}_b(k) = (1/2)[\boldsymbol{\alpha}_b(k-1) + (1/6)\Delta\boldsymbol{\phi}_b(k-1)] \times \Delta\boldsymbol{\phi}_b(k)$

3 - $\mathbf{v}_b(k) = \mathbf{v}_b(k-1) + \Delta\boldsymbol{\beta}_b(k); \mathbf{v}_b(0) = \mathbf{0}; \mathbf{v}_b(L) = \mathbf{v}_{L,b}; \mathbf{v}_b(k)$ reset at every T_{int}-cycle. (Thrust velocity)

4 - $\mathbf{S}_{\alpha,b}(k) = \mathbf{S}_{\alpha,b}(k-1) + \Delta\mathbf{S}_{\alpha,b}(k); \mathbf{S}_{\alpha,b}(0) = \mathbf{0}; \mathbf{S}_{\alpha,b}(L) = \mathbf{S}_{\alpha L,b}; \mathbf{S}_{\alpha,b}(k)$ reset at every T_{int}-cycle.

$\Delta\mathbf{S}_{\alpha,b}(k) = \boldsymbol{\alpha}_b(k-1)T_{int} + (T_{int}/12)(5\Delta\boldsymbol{\phi}_b(k) + \Delta\boldsymbol{\phi}_b(k-1))$

5 - $\mathbf{S}_{v,b}(k) = \mathbf{S}_{v,b}(k-1) + \Delta\mathbf{S}_{v,b}(k); \mathbf{S}_{v,b}(0) = \mathbf{0}; \mathbf{S}_{v,b}(L) = \mathbf{S}_{vL,b}; \mathbf{S}_{v,b}(k)$ reset at every T_{int}-cycle.

$\Delta\mathbf{S}_{v,b}(k) = \mathbf{v}_b(k-1)T_{int} + (T_{int}/12)(5\Delta\boldsymbol{\beta}_b(k) + \Delta\boldsymbol{\beta}_b(k-1))$

6 - $\Delta\mathbf{v}_{scul,b}(k) = \Delta\mathbf{v}_{scul,b}(k-1) + \delta\mathbf{v}_{scul,b}(k); \Delta\mathbf{v}_{scul,b}(0) = \mathbf{0}; \Delta\mathbf{v}_{scul,b}(L) = \Delta\mathbf{v}_{scul-L,b}; \Delta\mathbf{v}_{scul,b}(k)$ reset at every T_{int}-cycle.

$\delta\mathbf{v}_{scul,b}(k) = (1/2)[(\boldsymbol{\alpha}_b(k-1) + (1/6)\Delta\boldsymbol{\phi}_b(k-1)) \times \Delta\boldsymbol{\beta}_b(k) + (\mathbf{v}_b(k-1) + (1/6)\Delta\boldsymbol{\beta}_b(k-1)) \times \Delta\boldsymbol{\phi}_b(k)]$

<div align="right">(Sculling correction)</div>

7 - $\Delta\mathbf{R}_{scrl,b}(k) = \Delta\mathbf{R}_{scrl,b}(k-1) + \delta\mathbf{R}_{scrlA,b}(k) + \delta\mathbf{R}_{scrlB,b}(k)$

$\Delta\mathbf{R}_{scrl,b}(0) = \mathbf{0}; \Delta\mathbf{R}_{scrl,b}(L) = \Delta\mathbf{R}_{scrl-L,b}; \Delta\mathbf{R}_{scrl,b}(k)$ reset at every T_{int}-cycle.

$\delta\mathbf{R}_{scrlA,b}(k) = \Delta\mathbf{v}_{scul,b}(k-1)T_{gyr} + (1/2)\{\boldsymbol{\alpha}_b(k-1) - (1/12)[\Delta\boldsymbol{\phi}_b(k) - \Delta\boldsymbol{\phi}_b(k-1)]\} \times [\Delta\mathbf{S}_{v,b}(k) - \mathbf{v}_b(k-1)T_{gyr}] +$

$+ (1/2)\{\mathbf{v}_b(k-1) - (1/12)[\Delta\boldsymbol{\beta}_b(k) - \Delta\boldsymbol{\beta}_b(k-1)]\} \times [\Delta\mathbf{S}_{\alpha,b}(k) - \boldsymbol{\alpha}_b(k-1)T_{gyr}]$

$$\delta R_{scrlB,b}(k) = (1/6)\{S_{v,b}(k-1) + (T_{gyr}/24)[\Delta\beta_b(k) - \Delta\beta_b(k-1)]\} \times \Delta\phi_b(k) -$$
$$- (1/6)\{S_{\alpha,b}(k-1) + (T_{gyr}/24)[\Delta\phi_b(k) - \Delta\phi_b(k-1)]\} \times \Delta\beta_b(k) +$$
$$+ (T_{gyr}/6)\{\alpha_b(k-1) - (1/6)[\Delta\phi_b(k) - \Delta\phi_b(k-1)]\} \times \{v_b(k-1) - (1/6)[\Delta\beta_b(k) - \Delta\beta_b(k-1)]\} -$$
$$- (T_{gyr}/2160)[\Delta\phi_b(k) - \Delta\phi_b(k-1)] \times [\Delta\beta_b(k) - \Delta\beta_b(k-1)]$$

(Scrolling correction)

Intermediate speed computations at T_{int}-cycle rate
($T_{nav}/T_{int} = M$, k=1,2,...,M, k reset at every T_{int}-cycle)

8 - $D_{b(k-1)}^{b(k)}(k) = I + (1 - |\phi_{L,b}|^2/3! + |\phi_{L,b}|^4/5!)[\phi_{L,b}] + (1/2 - |\phi_{L,b}|^2/4! + |\phi_{L,b}|^4/6!)[\phi_{L,b}][\phi_{L,b}]$ (Incremental body rotation)

$$\phi_{L,b}(k) = \alpha_{L,b} + \gamma_{L,b}$$

9 - $D_{l^-}^{b(k)}(k) = D_{l^-}^{b(k-1)}(k-1)D_{b(k-1)}^{b(k)}(k)$; $D_{l^-}^{b(M)}(M) = D_{l^-}^{b}$; $D_{l^-}^{b(0)}(0) = D_{l}^{b}$ from previous T_{nav}-cycle.   (Incremental attitude update)

$$\zeta_{l^-l(k)}(k) = \Omega_{l^-} k T_{int} + \begin{bmatrix} \{\Delta R_{l^-b(k),l(k)}(k) \cdot [0\ 1\ 0]^T\}/[h(l^-) + R_E(l^-)] \\ \{-\Delta R_{l^-b(k),l(k)}(k) \cdot [1\ 0\ 0]^T\}/[h(l^-) + R_N(l^-)] \\ k T_{int} \rho_{l^-} \cdot [0\ 0\ 1]^T \end{bmatrix};\ \zeta_{l^-l(0)}(0) = 0$$

$$D_{l(k)}^{l^-}(k) = I - (1 - |\zeta_{l^-l(k)}|^2/3! + |\zeta_{l^-l(k)}|^4/5!)[\zeta_{l^-l(k)}] + (1/2 - |\zeta_{l^-l(k)}|^2/4! + |\zeta_{l^-l(k)}|^4/6!)[\zeta_{l^-l(k)}][\zeta_{l^-l(k)}]$$ (Incremental local level rotation)

10 - $\Delta R_{rot,b}(k) = [(1/3! - |\alpha_{L,b}|^2/5! + |\alpha_{L,b}|^4/7!)I + (1/4! - |\alpha_{L,b}|^2/6! + |\alpha_{L,b}|^4/8!)[\alpha_{L,b}]][S_{\alpha L,b} \times v_{L,b} + \alpha_{L,b} \times S_{vL,b}]$

11 - $\Delta R_{f,b}(k) = S_{vL,b} + \Delta R_{rot,b}(k) + \Delta R_{scrl-L,b}$ (Thrust position increment, compensated for sculling and velocity rotation)

12 - $\Delta R_{f,l}(k) = -(1/3)[\zeta_{l^-l(k)} - \zeta_{l^-l(k-1)}]\Delta v_{f,l^-}(k)T_{int} + D_{l(k-1)}^{l^-}D_{l^-}^{b(k-1)}\Delta R_{f,b}(k)$ (Local-level representation, compensated thrust position increment)

$$\Delta v_{f,l^-}(k) = D_{l^-}^{b(k-1)}\Delta v_{f,b(k-1)}(k)$$ (Local-level representation, thrust velocity increment compensated for sculling and velocity rotation)

$$\Delta v_{f,b(k-1)}(k) = v_{L,b} + \Delta v_{rot,b} + \Delta v_{scul-L,b}$$

$$\Delta v_{rot,b}(k) = (1/2! - |\alpha_{L,b}|^2/4! + |\alpha_{L,b}|^4/6!)(\alpha_{L,b} \times v_{L,b}) + (1/3! - |\alpha_{L,b}|^2/5! + |\alpha_{L,b}|^4/7!)[\alpha_{L,b} \times (\alpha_{L,b} \times v_{L,b})]$$

$$\Delta R_{l^-b(k),l(k)}(k) = \begin{cases} T_{int}\{(3/2)U_l(0) - (1/2)U_l(-1)\} & \text{para } k = 1 \\ T_{int}\{(3/2)U_l(k-1) - (1/2)U_l(k-2) + (1/2)\sum_{i=1}^{k-1}[U_l(i) + U_l(i-1)]\} & \text{para } k = 2,...,M \end{cases}$$

13 - $\Delta R_l(k) = T_{int}[U_l(k-1) + (1/2)\Delta v_{g/coriol,l}(k)] + \Delta R_{f,l}(k)$ (Incremental position change)

$$U_l(k^-) = U_l(k-1) + (1/2)[U_l(k-1) - U_l(k-2)]$$

$$\Delta v_{g/coriol,l}(k) = T_{int}\{g_{l^-} - [2\Omega_{l^-} + \begin{bmatrix} V_E(k^-)/[R_E(k^-) + h(k^-)] \\ -V_N(k^-)/[R_N(k^-) + h(k^-)] \\ \rho_{l^-} \cdot [0\ 0\ 1]^T \end{bmatrix}]U_l(k^-)\}$$ (Local level velocity increment due to gravity and Coriolis acceleration)

14 - $U_l(k) = U_l(k-1) + \Delta v_{g/coriol,l}(k) + \Delta v_{f,l}(k)$; $U_l(0)$ given   (Ground velocity update)

$$\Delta v_{f,l}(k) = D_{l(k)}^{l^-}\Delta v_{f,l^-}(k)$$

Slow speed computations at T_{nav} rate
(k=1,2,3,4...)

15 - $D_{l(k)}^{l(k-1)}(k) = I - (1 - |\zeta_{l^-l}|^2/3! + |\zeta_{l^-l}|^4/5!)[\zeta_{l^-l}] + (1/2 - |\zeta_{l^-l}|^2/4! + |\zeta_{l^-l}|^4/6!)[\zeta_{l^-l}][\zeta_{l^-l}]$ (Local level rotation update)

$$\zeta_{l^-l}(k) = \Omega_{l^-} T_{nav} + \begin{bmatrix} \{\sum_{j=1}^{M} \Delta \mathbf{R}_1(j) \cdot [0\ 1\ 0]^T\}/[h(l^-)+R_E(l^-)] \\ \{-\sum_{j=1}^{M} \Delta \mathbf{R}_1(j) \cdot [1\ 0\ 0]^T\}/[h(l^-)+R_N(l^-)] \\ \boldsymbol{\rho}_{l^-} T_{nav} \cdot [0\ 0\ 1]^T \end{bmatrix}$$ (Local level rotation)

$$\mathbf{D}_l^b(k) = \mathbf{D}_{l(k)}^{l(k-1)}(k)\mathbf{D}_{l^-}^b \ ; \quad \mathbf{D}_l^b(0) \text{ given by initial alignment procedure.}$$

16 -
$$\begin{bmatrix} \Lambda(k) \\ \lambda(k) \\ \Delta h(k) \end{bmatrix} = \begin{bmatrix} \Lambda(k-1) \\ \lambda(k-1) \\ \Delta h(k-1) \end{bmatrix} + \begin{bmatrix} \Delta R_E(k)/\{[R_E(k-1)+h(k-1)]\cos(\lambda(k-1))\} \\ \Delta R_N(k)/[R_N(k-1)+h(k-1)] \\ \Delta h(k)+s'(h(k-1)) \end{bmatrix}$$ (Position update in geographic coordinates)

$$[\Delta R_N(k)\ \Delta R_E(k)\ \Delta h(k)]^T = \begin{bmatrix} 1 & 0 & 0 \\ 0 & 1 & 0 \\ 0 & 0 & -1 \end{bmatrix} \sum_{j=1}^{M} \Delta \mathbf{R}_1(j)$$

4. - Results

Initially, the simulations assumed that sensors were perfect. The motivation was to validate the forced decoupling of strapdown navigation dynamics into a multirate scheme against a simultaneous integration approach (Waldmann, 2003b). Then, rate gyro quantization was investigated, as seen later in more detail.

4.1 - Solving the Continuous-Time Navigation Equations

The fourth-order Runge-Kutta integration method available in Matlab/Simulink with a fixed time step $\delta t=10^{-3}$s was used to evaluate Bar-Itzhack's continuous-time version of the b-l multirate algorithm with specific force $\mathbf{f_b}$ and angular rate $\boldsymbol{\omega}_b^{bi}$ along the following reference trajectory (Bar-Itzhack, 1977):

$$V_N = V_E = -V_D = 300+100t\,[m/s] \qquad t \in [0,200]\,[s] \qquad \psi = \sin(2\pi t/300)+0.5\sin(2\pi t/1.7)[rd]$$
$$\theta = \sin(2\pi t/300)+0.5\sin(2\pi t/1.7+0.3)[rd] \qquad \phi = \sin(2\pi t/300)+0.5\sin(2\pi t/0.85)[rd]$$

departing from ITA's geographic coordinates $\lambda(0)=-23°12'$, $\Lambda(0)=-45°52'$, and $h(0)=600$m. The above Euler angles ψ, θ, and ϕ represent the yaw, pitch, and roll angles, respectively. The continuous multirate algorithm had its fast and intermediate rate computations reset every 10^{-2}s. The horizontal root sum of squares error (RSS) index at the end of the trajectory was used as a measure of accuracy. The simultaneous solution of the navigation equations yielded RSS=3.0×10^{-8}m, whereas the b-l multirate scheme yielded RSS=5.7×10^{-1}m. Though the error relative increase was significant, the latter was minor in comparison with the covered distance of about 3,200km. Still, it was one order of magnitude higher than RSS=2.7×10^{-2}m reported in (Bar-Itzhack, 1977) for the continuous b-e multirate computational scheme. The latter scheme obviated the need for assuming constant $\boldsymbol{\rho}(\mathbf{R},\mathbf{U})$ to yield linear differential equations (Bar-Itzhach, 1977, 1978; Waldmann, 2003a, 2003b) because ground speed dynamics was represented in the earth-fixed coordinate frame rather than in the local-level one as in the b-l scheme. Furthermore, there is no periodic reset in the b-e split computational scheme. Further investigation revealed that the b-l multirate scheme yielded RSS=6.8m with a reset interval of 10^{-1}s, but the error dropped to RSS=6.7×10^{-2}m with a reset interval of 10^{-3}s and a fixed time step $\delta t=10^{-4}$s. Hence, forcing the system dynamics into distinct time scales detrimentally affected the continuous-time solution; the loss of accuracy depended on the selected reset interval. Moreover, any significant reduction of the reset interval should be accompanied by an appropriate reduction of the time step δt. A functional analogy connects the slow computation cycle interval T_{nav} of the discrete-time multirate algorithm to the reset interval of its continuous-time counterpart. Similarly, the T_{gyr}-cycle acquisition period of incremental inertial data in the discrete domain relates with the time step δt used to solve the continuous-time problem. A reduction of T_{gyr}, however, was limited by sensor quantization effects as reported later on. As expected, a tradeoff exists between the desired navigation accuracy, expected vehicle movement, and available computational resources. Such factors should be carefully weighed when designing SDINS's for autonomous vehicles.

4.2 - Solving the Discrete-Time Navigation Equations

Since the degradation of the continuous-time multirate solution was minor in comparison with the covered distance, a further investigation was carried out to assess the impact of discretization, i.e., use of incremental inertial data $\Delta\boldsymbol{\beta}_b$ and $\Delta\boldsymbol{\phi}_b$, on the attained navigation accuracy. Three cases were investigated:

1 - The previous test trajectory was used with the inertial measurement unit (IMU) located at the vehicle's CM;

2 - The vehicle`s CM resting relative to the ground, and the body frame performing a coning motion relative to the local-level frame (Waldmann, 2003c);

3 - Body frame undergoing coning motion, and the vehicle`s CM moving relative to the ground according to:

$$V_N = 200\sin(2\pi t/1200)[m/s] \quad t \in [0,300][s] \quad V_E = 150\sin(2\pi t/1200)[m/s] \quad V_D = 5\sin(2\pi t/300)[m/s]$$

In the latter two conditions that contemplate coning, the following angular rate relative to the local-level reference frame was used to assess the influence of noncommutative finite rotations (Bortz, 1971) on navigation errors:

$$\boldsymbol{\omega}_b^{bl} = \begin{bmatrix} -\Omega_p\sin(\theta)\cos(\Omega_p t) & -\Omega_p\sin(\theta)\sin(\Omega_p t) & \Omega_p(\cos(\theta)-1) \end{bmatrix}^T; \quad \theta = \pi/2[rd]; \quad \Omega_p = \pi/6[rd/s]$$

where θ and Ω_p are the cone half-angle and the precession rate of body axis $\mathbf{z_b}$ about the local vertical, respectively. In the last two conditions with coning motion, the IMU was located 1m off the vehicle's CM along the $\mathbf{z_b}$ axis.

Table (2) - Discrete-time performance in case 1, IMU at the vehicle's CM, no quantization error. (NA - not available)

$T_{nav}[s]$	10^{-2}	10^{-2}	10^{-3}	10^{-3}
$T_{gyr}[s]$	5×10^{-4}	10^{-4}	5×10^{-4}	10^{-4}
Mult. B.-I. RSS[m]	145	102	94	22
Mult. Sav. RSS[m]	220	228	NA	22

In the discrete-time multirate scheme, inertial data samples were acquired and body-frame thrust velocity $\mathbf{V_{f,b}}$ dynamics solved at the fast computation cycle T_{gyr}. $\mathbf{U_{g,l}}$ evolved in the intermediate time scale characterized by T_{int}-cycle period. At the end of each slow T_{nav}-cycle, $\mathbf{V_{f,b}}$ was reset to zero and $\mathbf{U_{g,l}}$ to the updated $\mathbf{U_l}$, as shown in Table (1).

Table (3) - Discrete-Time Performance - cases 2 and 3, IMU off the vehicle's CM, no quantization error.

	Vehicle`s CM at rest		Vehicle`s CM in motion		
$T_{nav}[s]$	9.996×10^{-2}	9.996×10^{-2}	9.996×10^{-2}	9.996×10^{-2}	9.996×10^{-3}
$T_{gyr}[s]$	8.33×10^{-3}	8.33×10^{-4}	8.33×10^{-3}	8.33×10^{-4}	8.33×10^{-4}
Mult. B.-I. RSS[m]	17	1.7	65	15	9
Mult. Sav. RSS[m]	1.4	1.0	26	26	3.4

Tables (2) and (3) indicate the impact of incremental inertial data and discretization error on navigation accuracy for both Savage's and Bar-Itzhack's multirate algorithms. The navigation error was reduced at the expense of a heavier computational burden, i.e., by decreasing T_{nav}, the analogue of the continuous-time reset interval. Further improvement resulted from a suitable reduction of T_{gyr}, a step analogous to reducing the fixed-time step δt used to solve the continuous-time equations. A higher data acquisition rate better captured motion dynamics, and thus improved accuracy. No relevant change in performance resulted from varying T_{int}. Table (2) shows that, for the b-l multirate scheme with $T_{nav}=10^{-3}$s, accuracy was much improved after the fast cycle T_{gyr} was reduced from 5×10^{-4}s to 10^{-4}s. The error at the end of the trajectory, though much larger than in the continuous-time solution, was not significant relative to the distance traversed by the vehicle. Table (3) shows that Savage´s approach, with its complex coning, sculling, and scrolling compensation terms, yielded the most accurate results. Errors of comparable magnitude, however, were produced as *both* T_{nav} and T_{gyr} were reduced. An adequate *balance* between the reset interval and data acquisition rate is called for because navigation accuracy improves by means of a faster data acquisition though at the expense of more computer throughput.

Figure (1) depicts the evolution of the horizontal RSS error that resulted from Bar-Itzhack´s multirate scheme in condition 2 in comparison with the simultaneous integration of the navigation equations under the assumption of constant specific force over the T_{nav} interval. The high-frequency fluctuation is caused by the computation of the horizontal RSS error at the IMU location relative to the vehicle's CM. Figure (2) shows the corresponding horizontal errors. Figure (3) presents the reduction of RSS error that resulted from increasing the data acquisition rate, and the corresponding improved accuracy in the horizontal plane. Figure (4) depicts for case 3 the effect of varying the reset

interval T_{nav} without changing the data acquisition interval $T_{gyr}=T_{nav}/N$. Clearly, in comparison with case 2, the CM's motion relative to the ground affected the navigation accuracy.

Figure (1) - Horizontal RSS error in case 2: a comparison between the b-l multirate scheme and simultaneous integration of the navigation equations assuming constant specific force over interval $T_{nav}=0.09996$s. $T_{gyr}=T_{nav}/12$, and $T_{int}=T_{nav}/4$.
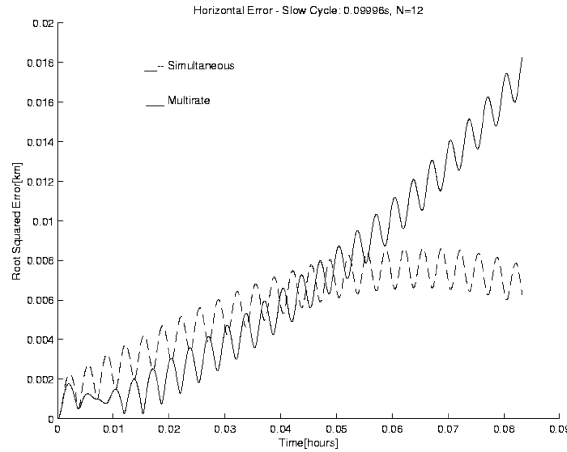

Figure (2) - Horizontal error in case 2: simultaneous integration on the left, and the b-l multirate algorithm on the right.
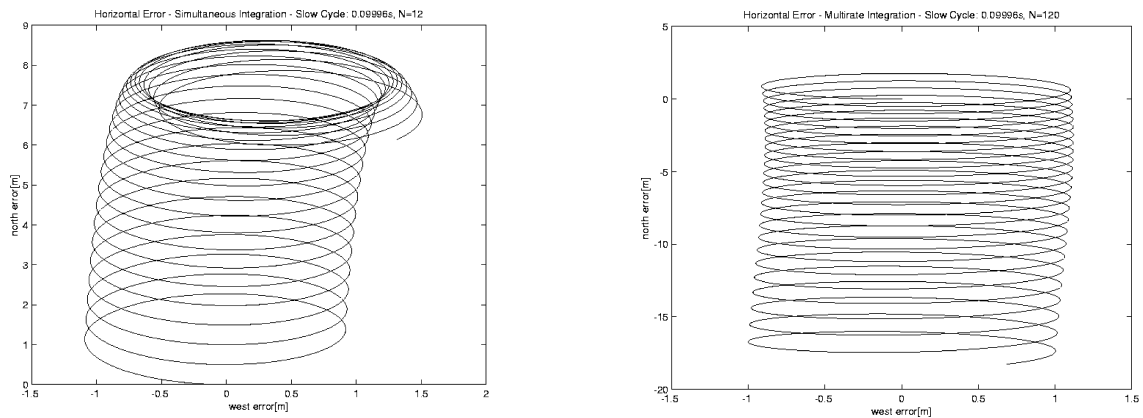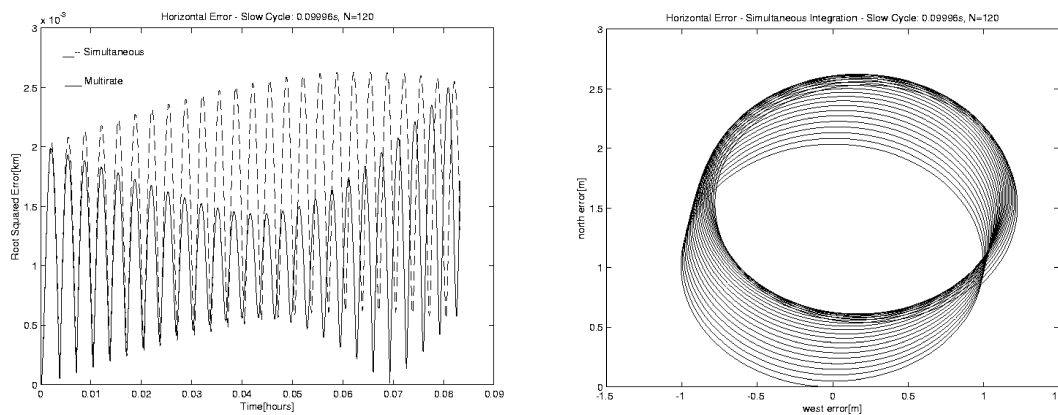

Figure (3) - Horizontal RSS error in case 2: on the left, a comparison between the b-l multirate scheme and simultaneous integration of the navigation equations; on the right, the corresponding horizontal error. $T_{nav}=0.09996$s, $T_{gyr}=T_{nav}/120$, and $T_{int}=T_{nav}/40$.

The previous results, obtained assuming use of perfect sensors show that increasing the acquisition rate improves navigation accuracy. In practice, quantization corrupts sensor output. The following question is posed: as sensor acquisition rate is raised, how is navigation accuracy affected by sensor quantization? Figure (5) shows results

concerning the effect of rate gyro quantization on navigation errors for both multirate schemes in case 1. According to Musoff (1995) Fig.4, for coning motion and 1μrd (approximately 0.21arcsec) rate gyro incremental output quantization, attitude determination drift increased one order of magnitude when the sampling rate increased from 100Hz to 300Hz. Recently, it has been contended that differentiation of white noise, though mathematically incorrect, provided a meaningful model of how rate gyro quantization affected the navigation accuracy (Savage, 2002). According to Eqs. (71) and (72) in that reference, the white process noise spectral densities in the error propagation equations are inversely proportional to raising the slow, intermediate, and fast computational rates by the same factor. An hypothetical situation with a rate gyro pulse size of 1arcsec was analyzed to provide evidence in favor of the white noise differentiation model to describe incremental angle quantization in comparison with the usual assumption of random walk. In this regard, from the Conclusions section, one reads (Savage, 2002):

"In general, for proper quantization modeling, the higher the frequency, the smaller is the effect of quantization error. Mismodeling can falsely lead to the opposite conclusion, that is, higher update frequencies increasing quantization error contributions."

Figure (4) - Effect of varying T_{nav} on the horizontal RSS error in case 3: on the left, the b-l multirate scheme, and on the right, the corresponding horizontal error.
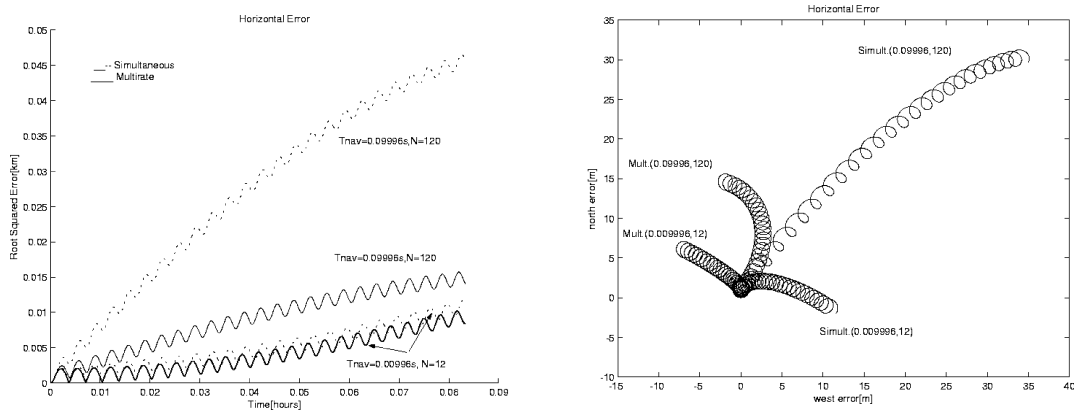

Figure (5) shows how navigation accuracy with 1arcsec quantization degraded after raising the intermediate and fast cycle update frequencies f_{gyr} and f_{int}, respectively, by the same factor from $f_{gyr}=500Hz$ and $f_{int}=200Hz$ to $f_{gyr}=4kHz$ and $f_{int}=1.6kHz$ in both Bar-Itzhack's and Savage's multirate schemes. Such results are in disagreement with the analysis carried out in Savage (2002) and contradict the conclusion quoted above. On the other hand, with 0.1arcsec quantization some improvement was observed - though minor in Savage's approach, thus contradicting results from Musoff (1995). Hence, besides lacking a sound mathematical background because white noise is nondifferentiable, the simulation results show that Savage's quantization-induced error model does not capture the impact of sensor quantization on navigation accuracy. The interaction among sensor quantization level, sensor sampling and processing frequency, and navigation accuracy deserves further theoretical investigation accompanied by validation.

Figure (5) - Rate-gyro quantization-induced navigation error behavior as a function of multirate update frequencies: Bar-Itzhack's b-l scheme on the left, and Savage's on the right.
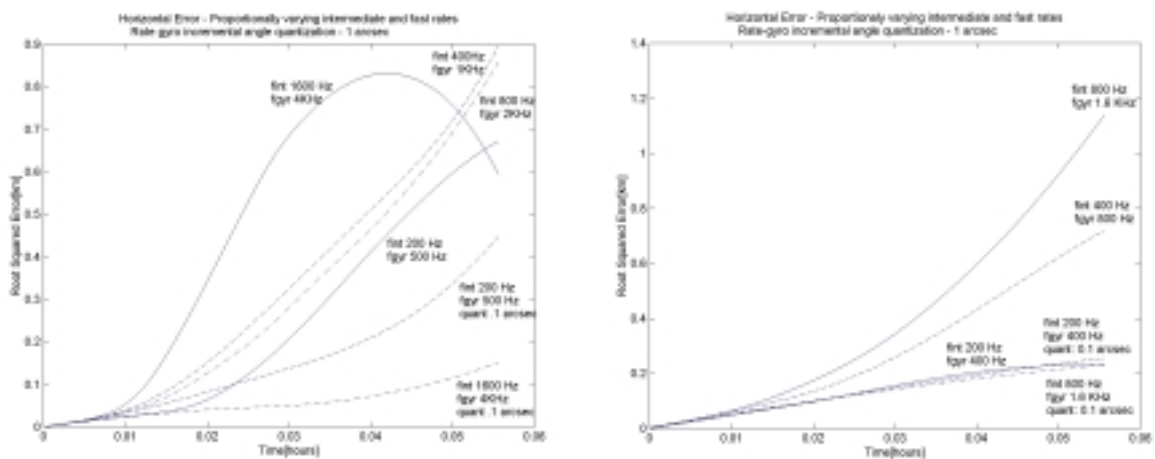
Conclusion

The existence of limited computational resources in autonomous vehicles strongly motivates the investigation of multirate terrestrial strapdown navigation algorithms. Initially, simulations with ideal sensors were carried out to compare the performance of a variation of Bar-Itzhack's b-l split coordinate multirate computational scheme, simultaneously integrating the navigation equations, and Savage's approach to sculling and scrolling. The latter providing the most accurate results at the cost of significant complexity. Bar-Itzhack´s elegant approach showed an acceptable balance between accuracy and simplicity in the investigated conditions.

An analogy was found between the reset interval in the continuous-time solution and the largest computation interval T_{nav} used to update position estimates in the discrete-time domain. Likewise, the time step used to solve the continuous-time algorithm and the data acquisition interval in the discrete domain had a similar impact on navigation accuracy. The latter similarity, however, was significantly affected by rate gyro output quantization. A balance between the reset interval (i.e., the slow T_{nav} position update cycle) and sensor acquisition rate (i.e., the fast T_{gyr} inertial data processing and attitude update cycle) should be found subject to the available computational resources on board, and consideration of sensor characteristics, expected kinematics and maneuverability from the vehicle, and desired navigation accuracy. In spite of the forced dynamical separation and the very distinct assumptions employed in both multirate schemes by Bar-Itzhack and Savage, the latter yielded more accurate results yet comparable to the former. The results presented here are valuable in the design of miniature autonomous vehicles expected to accomplish navigation by purely inertial means for brief periods of time and relying on limited computational resources on board.

5. References

Bar-Itzhack, I. Y., 1977, "Navigation Computation in Terrestrial Strapdown Inertial Navigation Systems," IEEE Transactions on Aerospace and Electronic Systems, Vol.13, No.6, pp.679-689.

Bar-Itzhack, I. Y., 1978, "Corrections to "Navigation Computation in Terrestrial Strapdown Inertial Navigation Systems"," IEEE Transactions on Aerospace and Electronic Systems, Vol.14, No.3, pp.542-544.

Bortz, J. E., 1971, "A New Mathematical Formulation for Strapdown Inertial Navigation," IEEE Transactions on Aerospace and Electronic Systems, Vol.7, No.1, pp.61-66.Kokotovic, P. V., O'Malley, R. E., and Sanutti, P., 1976, "Singular perturbations and order reduction in control theory: an overview," Automatica, Vol.12, pp.123-132.

Litmanovich, Y.A., Lesyuchevsky, V.M., and Gusinsky, V.Z., "Two New Classes of Strapdown Navigation Algorithms," Journal of Guidance, Control, and Dynamics, Vol.23, No.1, 2000, pp.34-40.

Mark, J.G., and Tazartes, D.A., "Tuning of Coning Algorithms to Gyro Data Frequency Response Characteristics," Journal of Guidance, Control, and Dynamics, Vol.24, No.4, 2001, pp.641-647.

Musoff, H., and Murphy, J. H., "Study of Strapdown Navigation Attitude Algorithms," Journal of Guidance, Control, and Dynamics, Vol.18, No.2, 1995, pp.287-290.

Savage, P.G., "Strapdown Inertial Navigation Integration Algorithm Design Part 2: Velocity and Position Algorithms," *Journal of Guidance, Control, and Dynamics*, Vol.21, No.2, 1998, pp.208-221.

Savage, P.G., "Analytical Modeling of Sensor Quantization in Strapdown Inertial Navigation Error Equations," Journal of Guidance, Control, and Dynamics, Vol.25, No.5, 2002, pp.833-842.

Stankovic, J.A., "Misconceptions About Real-Time Computing: A Serious Problem for Next-Generation Systems," *Computer*, Vol.21, No.10, 1988, pp.10-19.

Waldmann, J., 2002, "Relative quaternion discrete-time algorithm for terrestrial navigation with strapdown inertial sensors," Proceedings of the XIV Brazilian Congress on Automation, Natal, Rio Grande do Norte, Brazil, pp.2361-2366.

Waldmann, J., 2003a, "Forced singular perturbations as theoretical background to a split-coordinate frame multirate strapdown terrestrial navigation algorithm," Proceedings of the ICCA'03 Fourth International Conference on Control and Automation, Montreal, Canada, pp.28-32.

Waldmann, J., 2003b, "Forced singular perturbations in multirate terrestrial strapdown navigation," accepted for publication in the COBEM03 17th International Congress on Mechanical Engineering, São Paulo, São Paulo, Brazil.

Waldmann, J., 2003c, "An alternative derivation of classic coning motion via Euler angles," submitted to the COBEM03 17th International Congress on Mechanical Engineering, São Paulo, São Paulo, Brazil.